AUTOPSY OF REFRACTORY LINING IN ANODE KILNS WITH OPEN AND CLOSED DESIGN

Trond Brandvik[1], Zhaohui Wang[1,2], Arne Petter Ratvik[2] and Tor Grande[1]

1. Department of Material Science and Engineering, NTNU Norwegian University of Science and Technology, Trondheim, Norway

2. SINTEF Materials and Chemistry, Trondheim, Norway

Abstract

Aluminosilicate refractory lining constitutes a major part of anode baking kilns, and during anode baking the lining is exposed to harsh conditions which limits the lifetime. Here, autopsies of refractory linings from both an open and closed top furnace are reported aiming to determine microstructural and mineralogical changes in the lining during operation. Significant variations in density and porosity were observed, both across the brick cross sections, but also for the vertical position in the lining. The chemical and mineralogical composition of the bricks were investigated by electron microscopy and X-ray diffraction. Only minor changes in the mineralogical composition of the materials were observed, and sodium originating from green anodes were only observed to a minor degree. Evidence of silicon oxide transport from the lower to the upper part of the linings were observed, reflecting the changes in reducing-oxidizing conditions during an anode baking cycle. The main degradation mechanisms in these linings were due to densification of the material over time, particularly the uneven densification across a lining wall. The present findings are discussed and related to the main differences in the two furnace designs.

Introduction

The production of primary aluminum is carried out through electrolytic reduction of dissolved alumina in a fluoride electrolyte with carbon oxidation as the complementary anode reaction (1,2). The dominating anode technology today is prebaked carbon anodes due to the superior properties compared to Søderberg anodes (3,4). The green anodes are made of a mixture of petroleum coke, recycled anode butts and coal tar pitch, which are subjected to heat treatment (baking) in anode baking furnaces (2). The fabrication of prebaked carbon anodes is

fairly similar from plant to plant, however with the furnace design having two major configurations; i.e. open and closed top (1,5,6). The main construction element in the anode baking furnace is the refractory flue wall, which separates the anodes from the flue gas during operation. The flue walls consist mostly of alumina and silica, with some variations in alumina to silica ratio. Due to the harsh operational conditions in the furnace during baking, the refractory flue walls degrade over time (1,5–7). One contributor to this degradation is the thermal cycling, ranging from room temperature to 1200 °C in each baking cycle lasting ~14-17 days, giving rise to thermal induced stress. In addition, the gaseous environment surrounding the refractories at the anode side may also contribute. Green anodes are made of 20-25 % recycled anode butts, which contains traces of the electrolyte and impurities like Na and F. The presence of cryolite will cause volatile species like NaF and $NaAlF_4$ to form during baking, which may react with the refractory materials resulting in degradation of the wall (1,7–10). Typically, CO, CH_4, H_2, as well as other hydrocarbons, are formed during baking, either from the coke itself or the coal tar pitch. These reducing gaseous species may cause reduction of the aluminosilicate lining (1,7,8). To be able to absorb thermal expansion during heating, the flue wall is made with mortar-filled gaps between the bricks allowing some flexibility as the temperature cycles. Volatile hydrocarbons are likely to crack at the hot flue wall resulting in carbon deposition filling the gaps and thus reducing the walls' flexibility. This will result in a reduction in the walls' ability to absorb thermal expansion and hence an increase in the development of thermal stress during baking.

The aim of this work was to investigate the degradation of the refractory lining in anode baking furnaces. In order to address the differences between the open and closed furnace design, two autopsies were carried out with focus on changes in the mineralogy, microstructure and density in both flue walls. Preliminary data from the first autopsy have been reported earlier (11), and the study is in this report continued to include an additional autopsy and extended microstructure and mineralogical characterization. Finally, a thorough discussion with respect to possible degradation mechanisms and differences between open and closed top furnace is presented.

The anode baking furnace

The baking furnaces are in general designed as a ring pit furnace, where the individual sections are connected in series. Each section is divided into several pits, where the pits are separated from each other by the refractory flue walls. A typical pit is 5 m deep, 5 m long and 1 m wide. The flue gas is flowing inside hollow flue walls allowing for heating of the furnaces by combustion. The green anodes are placed in the pits and covered with packing coke to prevent anode oxidation during baking (12). Heating is performed by burners fueled with typically natural gas,

LPG or oil, which are moved around the furnace in fire trains (the part of the furnace where the heating occurs). A typical fire train covers eight sections, where three are assigned to preheating, three to maximum temperature baking, and the two at the end are assigned to cooling. As the train moves one section every 22-28 hours, the anodes in a given section will first be preheated for three periods, then baked at maximum temperature, before cooled down to room temperature. There are usually two to three fire trains moving around the furnace, leaving several unoccupied sections between each train available for anode replacement and furnace maintenance. During the first part of the baking cycle, volatile hydrocarbons evaporate from the green anodes and are combusted in the flue gas as the temperature increases, contributing to the overall heat input to the furnace. The main structural difference between the open and closed furnace design is the section covers used in the closed design. The flow of hot flue gas through the furnace is affected by the use of section covers, thus the flue gas flow pattern is varying between the two furnace designs and subsequently affecting the operational environment in the furnace during baking.

Open top furnace design

The open top baking furnace does not have section covers. The anodes are thus not separated from the surrounding atmosphere, emphasizing the need for packing coke to avoid anode oxidation during baking. Without a section cover, the flue wall itself must be sealed in order to keep the hot gas within the flue. The flue walls in the open top furnace are thus constructed as hollow two-layered refractory walls, where the flue gas is inside each wall. A section from an open top furnace is illustrated in **Figure 1a**. The cross section of the flue wall shows the flow direction of the flue gas as illustrated by arrows. Within the flue wall there are baffles and tie bricks controlling the flow pattern of the flue gas, in addition to giving the wall mechanical stability (12). The open arrangement of the pits dictates that the vapors released from the anodes must be sucked through the flue walls to avoid harmful release to the working environment. This is achieved by reducing the pressure within the flue walls. The two-layered flue wall lining has a width of 10-12 cm, which differs significantly from the closed top design.

Closed furnace design

The closed top furnace design utilizes section covers to close off the sections that are being subjected to heat treatment. The sections are thus more or less sealed towards the working environment during baking resulting in better control of the atmosphere within the section. The flue walls used in this design are made by a single-layered, hollow refractory wall, where the flue gas flows within channels in the wall. A section of a closed baking furnace is illustrated in **Figure 1b**. The cross section shows the two parts of the flue wall, defined by how each part leads

the flue gas. In part A the flue gas enters the wall at the bottom and is transported upwards through the channels in the wall. At the top of the flue wall, the flue gas is released underneath the section cover, before being transported down by the reduced pressure in part B. The flue gas outlet is in the bottom right corner of part B where the gas is transported into part A of the next section. The flue wall arrangement is varying to some extent between different closed furnaces, but the overall design concept is the same. The lining in this design is 4-5 cm thick, significantly thinner compared to the open top furnace design.

Experimental

Autopsy

Samples from spent refractory lining from anode baking furnaces with both open and closed top design were collected, after approximately 160 and 63 cycles in operation, respectively. From the furnace with open top design, sampling were performed at three heights: top, middle and bottom, where the top layer was collected ~1 m below the top of the flue wall. The closed top furnace design has two sections of the refractory wall (part A and B), where each part were sampled at three heights, similarly as for the open top furnace. **Figure 2** shows the cross section of the refractory bricks used in the closed (a) and the open (b) top designs, illustrating the differences in width. In order to investigate structural and mineralogical changes as a function of distance from the anode side, all samples were cut into smaller sections with the size of 1-2 cm^3. Due to the difference in width of the refractory lining in the two furnaces, the division into the smallest sections varied as shown in **Figure 2**. Samples from the open top design were divided into eight smaller sections, while samples from the closed top design were divided into four or five sections. All samples were polished down to 1 µm prior to further characterization by microscopy. If otherwise is not explicitly stated, the results are referring to the polished samples. Some investigations were also conducted on fracture surfaces. X-ray diffraction were performed using powders obtained by grinding with a Herzog HSM pulverizing mill in a WC vessel, before subsequent sieving to < 63 µm.

Material characterization

The as-cut samples were analyzed with respect to apparent density and open porosity by the Archimedes' method as described in ISO5017 using water as immersion liquid. The weight difference after heat treatment at 1150 °C for 48 hours in air were determined gravimetrically in order to quantify the amount of deposited carbon in the open porosity. The qualitative phase composition of the samples was investigated by powder X-ray diffraction

using a Bruker D8 DaVinci diffractometer with a LynxEye SuperSpeed detector and CuKα radiation. Microstructural and chemical analysis was carried out with a Zeiss Supra 55 VP field emission scanning electron microscopy, with the associated energy dispersive X-ray spectroscopy (EDS). X-ray fluorescence (XRF) analysis was done by a Bruker S8 Tiger 4 kW X-ray diffractometer.

Results

Pristine composition and microstructure of the refractory bricks

The refractory materials in both furnaces are similar in microstructure prior to service. In **Figure 3**, the microstructure of the pristine refractory material from the open baking furnace is presented. The microstructure is in general heterogeneous with a broad particle size distribution and a significant level of open porosity. The chemical compositions of the two materials determined by XRF is presented in **Table 1**, demonstrating the similarities of the two materials with respect to chemical composition. The sodium content of both materials is below the XRF detection limit of 0.02 wt% Na_2O. (**Table 1.**).

A typical phase composition of the pristine materials from both furnace designs is presented in **Figure 4c**. The main phases present in the materials from the open furnace lining are mullite ($Al_6Si_2O_{13}$) and cristobalite (SiO_2). The brick from the closed furnace consists of comparable levels of mullite, significantly lower cristobalite content and minor amount of andalusite (Al_2SiO_5), which remains from the raw materials used.

Phase composition of spent lining

X-ray diffraction patterns of the anode facing samples from both furnaces are presented in **Figure 4a and 4b**. In general, there are no major variations with respect to phase composition in the materials of either of the two linings. The open top furnace samples (**Figure 4a)** consist of mullite and cristobalite, with a relatively constant mineralogical composition. The largest variation is observed with respect to cristobalite, being especially evident for the reflections at ~21.9°. The phase transition between α-cristobalite, the stable polymorph at ambient conditions, and β-cristobalite is reported between 170 °C and 270 °C, dependent on defects or strains (13–15). The X-ray diffractograms demonstrate the presence of both α- and β-cristobalite in various amounts. Suppression of the β- to α-cristobalite transition have been investigated and it can be effected by solid solution of other oxides in the crystal structure (14–16). The ratio of α- to β-cristobalite in the samples is varying, but there is no clear trend with respect to vertical position or distance from the anode. X-ray diffractograms for the closed furnace

show the similar observations regarding the content of α- and β-cristobalite (Figure 4b). Andalusite is observed in addition as in the pristine material, and the content of this phase is changing, having a higher intensity in the top section, compared to the middle and bottom sections. Finally, it is worth pointing out that there is no evidence for the presence of significant amounts of an amorphous phase in either of the linings based on X-ray diffraction.

Visual investigations of spent lining

Optical images of the cross section of the flue wall from both the closed and open anode baking furnace are shown in **Figure 2**. The as-cut cross sections of the refractory material show clear indications of exposure to harsh environments during operation. Both linings have been exposed to the anodes at the left side, evident from the discoloring. Carbon deposition or reactions in the lining was suspected as one possible mechanism for the darkening of the region facing towards the anode. Heat treatment of samples at 1150 °C for 48 hours demonstrated significant weight loss close to the anode side, corresponding to combustion of deposited carbon as reported earlier (11). The color of the samples (not shown) did also change due to the thermal treatment in air, giving additional evidence that the discoloring is due to carbon deposition and partly reduction of the lining towards the anode side.

Density and microstructure of refractory lining in open top design

Apparent density and open porosity measured for the three sampling heights in the open top furnace are summarized in **Figure 5,** showing a distinct increase in density. The gray region corresponds to the distribution of the measured density of the unreacted pristine materials. The densification is more pronounced closer to the anode side, in addition to being significantly higher in the bottom of the furnace compared to the middle and top section. Close to the flue side, the density is converging towards the pristine material for all three sampling heights. Density were measured both before and after heat treatment, corresponding to the filled and open markers in **Figure 5**, respectively. The density is significantly reduced after heat treatment caused by removal of deposited carbon within the open porosity. The open porosity presented in **Figure 5** confirms the variation in the density, showing that the increase in the density is accompanied by a corresponding reduction in the open porosity.

The autopsy samples were thoroughly examined by electron microscopy, showing microstructural changes at the regions closest to the anode. This change in microstructure is mainly found in grains facing the anode pit directly, or in the vicinity of open pores. **Figure 6a** shows the characteristic needle-like microstructure observed in the degraded layer in the bottom section. The layer is varying in width, up to ~200 µm. EDS analysis demonstrated that the degraded area has a low silica content, i.e. there has been a depletion of silica from the refractory during operation. The remaining needle-like grains are composed of an aluminosilicate phase, close to mullite in

composition. This chemical wear is primarily observed in the middle and bottom section of the flue wall, whereas the top section shows far less chemical wear of this kind. In the top section, the microstructural changes are quite different compared to the middle and bottom sections. While there are few signs of chemical wear, grains with very high silica content are present. In **Figure 6b**, an EDS image of the top section shows that the level of silica (yellow) and alumina (purple) varies significantly in this section. The chemical composition of the regions labeled 1, 2 and 3 in **Figure 6b** are presented in **Table 2**. Region 1 has a high silica content, while Region 2 and 3 show varying chemical composition. The probing volume of the EDS is larger than each individual phase, and the EDS represent average compositions and not the composition of the mineral phases present in the material. The regions with high silica content are found all over the outer surface of the top section towards the anodes, both in the regions where the refractory wall is facing the anodes directly, including regions close to open porosity.

The microstructure of the outer regions of a spent brick is shown In **Figure 6c**, showing variation in atomic contrast close to the surface. The average chemical composition of region 4 and 5 is found in **Table 2**, demonstrating significantly higher alkali content in the lighter region closer to the surface. No evidence of fluorine anions were observed by EDS in any of the samples. Even though there is a significant higher sodium content in point 4 compared to point 5, the overall sodium content is low. The absence of an amorphous phase from the X-ray diffraction investigations corresponds well with the relatively low levels of sodium. Previous investigations of similar furnaces often showed a glassy layer with a high sodium content in the outer parts of the sample (7). This is not observed in any of samples from the spent lining.

Density and microstructure of refractory lining in closed top design

Spent lining density from the closed top furnace are presented in **Figure 7.** The density is also in this case higher compared to the pristine density, but there is no major difference between part A and part B. Some variation in densification is found within each part, where the top section are less affected by densification and has a lower density compared to the middle and bottom sections, which are relatively similar. It is important to note the difference in the width of bricks in the two furnace designs, 11 cm versus 4 cm, and the minor variations in the density of the closed furnace could be due to the relative narrow cross section. Within the 4 cm outer region in the open design shown in **Figure 4**, the variation in the density is comparable to the one shown in **Figure 7**. No significant reduction in density after heat treatment was observed.

The microstructural changes observed in the open top furnace are also found in the closed top furnace. Both depletion and deposition of silica are observed at various positions in the furnace. The chemically etched regions

with the needle-like microstructure and low silica content are also present in the closed furnace, but not as a continuous layers and mainly close to open porosity or the anode-facing surface. The deposition of near-spherical silica particles were observed similarly in the closed furnace as for the open furnace design. The systematic variations with respect to sampling height are however not found in the same manner. Both the chemical wear, silicon depletion and deposition were observed in the top and bottom section, and cannot be related to the vertical position in the wall as clearly as for the open furnace. The degree of chemical degradation is also less in the closed furnace compared to the open furnace, possibly reflecting the difference in the number of exposed baking cycles.

X-ray diffraction analysis demonstrate that there is a low content of amorphous phase in the closed furnace, similar as observed for the open furnace design. This corresponds with the overall low level of sodium found in the spent lining, and the absence of a glassy layer close to the anode. A phase with high amounts of Al, Ni and Fe was found in the top section of the closed furnace as shown in **Figure 8**. The phase was found in various amounts in the top section of both part A and part B. The average chemical composition of this phase is summarized in **Table 3**, marked as region 6.

Investigations of a fracture surface from the bottom lining of the closed furnace revealed precipitation of iron rich particles all over the surface, see **Figure 9**. The fracture, going from the anode side towards the flue side, was present prior to sampling startup and can thus have occurred during operation of the furnace. The composition of the lighter particles (region 7) and the background phases (region 8a and 8b) in **Figure 9** is summarized in **Table 3**. The particles have a high and stable content of Fe, while variation is observed for the material below the Fe-rich particles. In most cases the refractory is rich in silica although an aluminosilicate phase is also observed below the particles. At the same fracture surface, particles of almost pure silica were observed, while on top of these silica rich particles, a lighter phase was observed. Both phases are marked as region 9 and 10 in **Figure 9**, with the corresponding chemical composition given in **Table 3**.

Discussion

Densification mechanism

The observed changes in density and open porosity demonstrate significant changes in the microstructure of the refractory lining. The observed densification results in reduction of the porosity and dimensional changes of the bricks in the regions with densification. Refractory materials are designed to operate at high temperature

conditions, with the ability to withstand high temperature sintering or densification. This is achieved by the wide particle size distribution in the raw materials, where the largest particles give dimensional stability with smaller particles filling the voids. In order for densification to occur the center of particles must move closer towards each other, which is achieved by mass transport away from particle contact points. Due to the heterogeneous nature of the microstructure, a relative high amount of mass needs to be transported away from the contact points before significant densification can be accomplished, resulting in slow sintering kinetics. Hence, it is not likely that high temperature alone should account for the degree of refractory densification as presented in **Figure 5**. Addition of glass modifiers (e.g. Na, K or Ca) to the aluminosilicate refractory will however have a large impact on the thermal stability of the flue wall, increasing sintering kinetics significantly by enabling plastic deformation. The variations in densification presented in **Figure 5** demonstrate that the conditions for densification are varying across the flue brick, being more in favor closer to the anode side.

There is a general agreement in the literature that sodium and/or fluorine containing gas species are important factors in the degradation of refractory lining in anode baking furnaces (1,2,5,7,17,18). Green anodes usually consist of 20-25 % recycled anode butts, which, due to the exposure to cryolite during electrolysis, pose a potential source of sodium and fluorine in the furnace. At elevated temperatures, cryolite present in the green anodes can evaporate forming gaseous fluorides and possibly reduce the phase stability of the refractory lining (10). Common for most reactions between gaseous fluorides and aluminosilicates is the formation of a sodium aluminosilicate phase (albite or nepheline) in addition to gaseous SiF_4 (10). If any reaction between volatile fluorides and the lining have occurred, sodium aluminosilicates would be present in the lining. **Figure 6c** and **Table 2** show lining with significant variation in sodium content, where the highest sodium concentration is found closest to the surface. These regions with elevated sodium content are found close to open porosity or the refractory surface facing the anodes. If the elevated sodium content is to be linked directly to the density variations presented in **Figure 5**, clear variations in sodium content with respect to vertical sampling position are expected. This is however not observed, making it difficult to correlate variations in densification to the distribution of regions with increased sodium content.

The sodium levels presented in **Table 2** are quite low compared to earlier reports (1,7). Furthermore, the chemical composition in these regions are not corresponding to the expected sodium aluminosilicate phases. The formation of nepheline ($NaAlSiO_4$) and albite ($NaAlSi_3O_8$) is regarded as irreversible reactions, and once formed, the reaction products are not likely to disappear. In addition, the amount of amorphous phase in both linings is low. High levels of gaseous NaF or $NaAlF_4$ close to the anode side of the lining would have resulted in significant

increase in sodium level and presence of sodium containing phases. The lack of sodium aluminosilicates in the spent lining is therefore disregarding the importance of degradation due to volatile fluorides (10). The present data demonstrate clearly the minor effect of volatile fluorides in the pit atmosphere in the two furnaces investigated. Consequently, the cryolite level in the anode butts must have been low, indicating good cleaning routines and operational of the baking furnaces.

A reduction in densification is observed by post heat treatment, as presented in **Figure 5.** Parts of the overall densification observed for spent lining can thus be related to carbon deposition in the open porosity. Coal tar pitch from the green anodes evaporates during heating, resulting in an atmosphere with high level of various hydrocarbons. At higher flue wall temperatures, parts of the hydrocarbons are likely to crack at the refractory surface, especially in areas with low suction, leaving solid carbon at the surface and in the open porosity, and consequently increased density. The reduction in density after heat treatment in air confirmed oxidation of carbon, hence supporting the proposed carbon cracking reaction (1,2,9). The preliminary study confirmed the presence of carbon in the outer layers facing the anode pit, with a significant reduction in carbon level farther into the lining (11). This corresponds to investigations on similar samples showing carbon build-up on the flue wall (9). The overall stability of the flue wall during thermal cycling is maintained by the use of mortar-filled gaps in the wall. These gaps enables the refractories to expand as the temperature increases, without causing compressional stress in the lining. However, over the course of years in operation, the gaps are filled with fines from the packing coke and deposited carbon, resulting in reduced overall flexibility. As the wall stiffens, the wall's ability to absorb thermal expansion is reduced, causing increased thermal stress to build up within the wall.

Transport of SiO

Most reports agree on two reaction schemes being the main cause of the changes in the silicon oxide content, i.e. either a reaction with gaseous fluorides, or a reaction caused by reducing atmosphere (1,2,5,7,10,11,17,18). The lack of sodium aluminosilicate in the spent lining investigated here supports the minor influence of fluorides in the present two cases, disregarding the first alternative as the main mechanism. Low partial pressures of oxygen in combination with high temperature and compounds like CO, CH_4 or H_2, is proposed to have a destabilizing effect on the refractory oxide lining. In the bottom of the open furnace, reaction layers depleted of silica was observed. In order for SiO_2 to be removed from the lining, conditions favoring sufficiently high partial pressures of SiO must be present. As carbon is present at the flue wall through deposition and cracking of hydrocarbons from the anode, the material system describing the conditions at the lining is thus consisting of solid carbon and

silica, in addition to gaseous CO, CO_2, and SiO. The partial pressures of these compounds are all linked together and highly dependent on the temperature in the furnace. **Equations 1-3** describe the equilibriums reactions between these gas species and solid carbon and silica.

$$C\,(s) + CO_2\,(g) = 2CO\,(g) \qquad (1)$$

$$CO_2\,(g) = CO\,(g) + \tfrac{1}{2}\,O_2\,(g) \qquad (2)$$

$$SiO_2\,(s) = SiO\,(g) + \tfrac{1}{2}\,O_2\,(g) \qquad (3)$$

At isothermal conditions, the Gibbs phase rule show that the system only has one degree of freedom. Hence, by fixing one of the partial pressures, the remaining partial pressures can be calculated. The Boudouard reaction in **Equation 1** describes the equilibrium between solid carbon, CO and CO_2, which is shown in the top part of **Figure 10**. As long as carbon is present (and the system is in equilibrium), the ratio between p_{CO}^2 and p_{CO_2} is fixed as shown by the line in the upper section of **Figure 10**. By increasing this ratio and moving into the grey area, the gas mixture becomes unstable and solid carbon is precipitated. Based on **Equations 2 and 3,** partial pressures of O_2 and SiO at equilibrium are plotted as a function of the partial pressure of CO in the lower part of **Figure 10**, where the solid and dotted lines correspond to 1300 °C and 1000 °C, respectively.

At low p_{O_2}, the partial pressure of SiO becomes high enough to result in SiO_2 volatility at 1300 °C. The oxygen partial pressure is expected to be low in the bottom of the open furnace, and thus favor such conditions, explaining the observed silica depletion in the reaction layers. In the top section of the same furnace, particles of precipitated silica were observed at the surface of the lining facing the anodes. This suggests a transport of SiO(g) from the bottom or middle section upwards to the top section of the furnace, before re-oxidation into SiO_2. In the open baking furnace, the anodes are covered with a layer of packing coke in order to avoid oxygen intrusion in the top section. The air burn of packing coke is however not completely avoiding oxygen intrusion because of the lower temperature in the packing coke towards the top. Consequently, the partial pressure of oxygen is significantly higher in the top section compared to the bottom. An increase in oxygen pressure is accompanied by oxidation of SiO(g), resulting in precipitation of SiO_2 particles in the top section. The thermodynamics show that a transport of silica from the bottom section to the top section in the open furnace is possible considering local equilibrium in the lower and upper part. Investigations of similar samples have shown that both silica depletion and deposition could occur in the same region, given that the local conditions favor both reactions (9). In the closed furnace, on the other hand, oxygen intrusion is reduced by the use of section covers, resulting in a significantly lower oxygen partial pressure in the flue gas below the section covers, compared to the surrounding air. A similar gradient in

oxygen partial pressure in the pit is therefore not expected, corresponding with the lack of systematic depletion and deposition of silica with respect to vertical position. Silica reduction and re-oxidation were both observed in the top and bottom section indicating favorable conditions more locally and transport of silica occurring over shorter distances.

Metal oxide precipitates

The chemical composition of the particles presented in **Figure 8** are fundamentally different compared to the surrounding aluminosilicate material. The high content of iron and nickel cannot be rationalized by the nominal composition of the refractory material. It is therefore unlikely that the high concentration of metal cations is due to a redistribution of the trace elements in the pristine aluminosilicate refractory material. Furthermore, no significant reduction in metal content of green and baked anodes during baking is found, suggesting the anodes not being the source of Ni and Fe. The packing coke could be a potential source of both Fe and Ni, but no additional study was done to verify this suggestion. In **Figure 9**, the fracture surface is covered in particles with very high iron content. The density of precipitated particles decreases when moving into the refractory from the anode side, supporting the suggestion of precipitation from gaseous compounds in the pit atmosphere. Iron hydroxide could be a potential iron carrier compound in these conditions (19), but to identify the specific mechanism resulting in transport of these elements requires further studies and are beyond the scope of this investigation.

Importance of furnace design and flow pattern

In the open baking furnace, densification, silica depletion and deposition were observed systematically with respect to both vertical position and distance from the anode. Chemical wear was observed as uniform layers in the middle and bottom section of the lining, while silica deposition was found in the top section. The densification was more pronounced in the bottom section and decreasing upwards in the furnace, in addition to being most pronounced closer to the anode side for the whole lining. In the closed furnace observations was less systematic and not following the same trends. Chemical wear was observed in specific areas, and not as the uniform degraded layer found in the open furnace. The areas where silica depletion was observed were found both in the top and bottom section without any apparent global trend. With respect to gaseous attack, the main difference between the two furnace designs is the flow pattern of the flue gas. As illustrated in **Figure 1**, the flue gas in the open furnace flows within the flue wall, and is never in direct contact with the anode side of the flue wall. In the closed furnace, the flue gas is released under the section covers after it escapes part A of the flue walls and is subsequently transported into part B. The main driving force for gas transport inside the furnace is the pressure difference across

the flue walls (both furnaces) and between the anode pit and the area below the section covers (only closed furnace). The reduced pressure inside the flue walls results in a mainly sideways gas transport from the anode pit and into the walls. In the open furnace, this is the main method for gas transportation out of the anode pits. For the closed furnace, the section covers results in a reduced pressure above the packing coke, leading to a transport of anode pit gas upwards, in addition sideways into the flue walls. This variation in gas transport from the anode pit to the flue should have an impact on the degradation pattern. The absence of clear degradation trends with respect to the vertical position in the closed furnace could relate to the upwards transport of pit gas, reducing vertical variations in pit atmosphere. Both the degradation and silica deposition occurs in the top and bottom sections, possibly due to local conditions at the flue wall, rather than global trends over the whole flue wall. In the open furnace, the reduced pressure in the flue wall cause a horizontal transport of pit gas, and any variations in pit atmosphere could to a larger extent be maintained. However, the clear trend in silica depletion and deposition in the open furnace indicate some transport of gaseous SiO from the bottom or middle section to the top section. It is difficult of estimate how much of the reduced silica that actually is transported upwards, since some could have gone into the flue walls and deposited elsewhere. In addition, the temperature cycling influences the gas transport, and silica depletion and deposition, making the description of the mechanisms more complex.

Depletion and deposition of SiO_2 was observed to a much larger degree in the open furnace compared to the closed furnace. This is not unexpected, considering the difference in the number of baking cycles each flue wall has been exposed to. The samples from the open furnace have been 160 cycles in operation, while the samples from the closed furnace have been 63 cycles in operation. Nevertheless, both flue walls were taken out of operation due to reduced performance, i.e. reduced structural and mechanical integrity, indicating that the silica transport is not the governing mechanism for the overall reduction in thermomechanical properties of the flue walls. It is more likely that the density variations have a larger implication on the overall thermomechanical stability of the flue walls, and thus is the main reason for the reduction in overall performance of the flue walls.

The variation in density (**Figures 5 and 7**) have some important differences when comparing the open and closed furnace. The clear trends observed for the open furnace, both with respect to distance from the anode and the vertical position in the lining, are not found equally distinct in the closed furnace. There could be several reasons for this observation, where the different flow pattern for the flue gas being one of them. Another important difference between the two sets of samples are the cross sectional width separating the anode side from the flue side, which is about 1/3 for the closed furnace compared to the open furnace. The density variations observed for the first 4 cm in the open furnace are comparable to the variation in the density variations found in the closed

furnace, indicating that the mechanism governing the densification could be the same for both furnaces. A final major difference is the position of the burners used to control flue gas temperature. In the open furnace, the burners are positioned inside the flue walls, never being in direct contact with the atmosphere surrounding the anode side of the flue walls. Any residues from the combustion of fuel will not mix with the pit atmosphere, and therefore not affect any chemical processes going on at the refractory surface facing the anode side. In the closed furnace, on the other hand, the burners are located underneath the section covers and inside the fire shafts, being directly in contact with the pit atmosphere.

Conclusions

Autopsies of spent refractory linings in an open and a closed baking furnace have been carried out with focus on mineralogical and microstructural changes. The study has illustrated differences and similarities with respect to degradation patterns of the two furnace designs. In the open baking furnace, significant densification was observed, in addition to transport of silicon oxide from the bottom to the top section. Both phenomena show clear dependencies of vertical position in the lining and horizontal distance from the anode into the flue wall. Similar observations have been reported for the closed baking furnace, but the variations were not systematic with respect to the position. Thermodynamic considerations support formation of SiO(g) due to reducing atmosphere as the main mechanism for SiO_2 transport. The difference in flue wall design is suggested to be the main reason for the observed variations between the two furnaces. Anode gas is transported out of the pit both horizontally and vertically, due to a reduced pressure in the flue wall and below the section covers, respectively. The former is found in the open furnace while both is the case in the closed furnace, linking to the variations in observed degradation trends. The observed densification demonstrate a significant change in brick dimensions during operation, most likely being the main cause of the reduction in thermomechanical stability of the flue wall. Finally, no significant levels of sodium or fluorine were observed in either of the furnace linings, demonstrating that chemical attach due to traces of electrolyte in the green anodes were not taking place in these two cases.

Acknowledgements

Financial support from the Norwegian Research Council and the industrial partners Hydro Aluminium, Alcoa, Elkem Carbon and Skamol A/S through the project ”Reactivity of Carbon and Refractory Materials used in metal production technology” (CaRMa) is acknowledged.

References

1. Prigent P, Bouchetou ML. Gaseous corrosion of aluminosilicate efractories in anode baking furnaces used for aluminium produciton part 1. *Interceram*. 2009;58(2–3):121–6.

2. Prigent P, Bouchetou ML, Poirier J, Hubert P. The effect of the addition of fine andalusite particles in refractory bricks on gaseous corrosion. *JOM* 2008;60(5):58–63.

3. Moors EHM. Technology strategies for sustainable metals production systems: a case study of primary aluminium production in The Netherlands and Norway. *J Clean Prod*. 2006;14:1121–38.

4. Schwarz H-G, Briem S, Zapp P. Future carbon dioxide emissions in the global material flow of primary aluminium. *Energy.* 2001;26(8):775–95.

5. Prigent P, Bouchetou ML. Gaseous corrosion of aluminosilicate refractories in anode baking furnaces used for aluminium produciton part 2. *Interceram*. 2009;58(4):202–9.

6. Prigent P, Bouchetou ML, Poirier J. Andalusite: An amazing refractory raw material with excellent corrosion resistance to sodium vapours. *Ceram Int*. 2011;37(7):2287–96.

7. Brunk F. Corrosion and behavior of firecal bricks used in the flues of open anode baking furnaces. *Light Metals.* 1995;641–6.

8. Oumarou N, Kocaefe D, Kocaefe Y. Investigation of the refractory bricks used for the fl ue wall of the horizontal anode baking ring furnace. *Ceram Int*. 2016;42(16):18436–42.

9. Wang Z, Rørvik S, Ratvik AP, Grande T. Formation of carbon cuild-up on the flue wall of anode baking furnace. *Light Metals* 2017;1265–74.

10. Brandvik T, Ratvik AP, Grande T. Thermodynamic assessment of the chemical durability of refractory lining in anode baking furnaces. Proceedings 34th Conference and Exhibition ICSOBA Qubec City, Cananda, October 2016.

11. Brandvik T, Ratvik AP, Wang Z, Grande T. Investigations of spent refractory lining in an anode baking furnace. *Light Metals*. 2017;4:1281–8.

12. Becker FH, Goede F. Ring pit furnaces for baking of high quality anodes - an overview. *Aluminium*. 82. 2006;9.

13. Damby DE, Llewellin EW, Horwell CJ, Williamson BJ, Najorka J, Cressey G, et al. The alpha-beta phase transition in volcanic cristobalite. *J Appl Crystallogr*. 2014;(47):1205–15.

14. Perrotta AJ, Grubbs DK, Martin ES, Dando NR. Chemical stabilization of p-cristobalite. *J Am Ceram Soc*. 1989;72(3):441–7.

15. Alcala MD, Real C, Criado JM. A new "incipient-wetness" method for the synthesis of chemically stabililzed beta-cristobalite. *J Am Ceram Soc*. 1996;79(6):1681–4.

16. San O, Özgür C. Investigation of a high stable beta-cristobalite ceramic powder from CaO-Al_2O_3-SiO_2 system. *J Eur Ceram Soc*. 2009;29:2945–9.

17. Butter J, Bongers A. Alterations of anode baking furnace bricks during operation. *Light Metal.* 1995;633–9.

18. Uhrig JR. A unique refractory solution for anode baking furnace flues. *Light Metal*. 2004;553–7.

19. Belton GR, Richardson FD. A volatile iron hydroxide. *Trans Faraday Soc*. 1962;58(1):1562.

Table 1: Chemical composition of the pristine refractory material used in the open and closed baking furnace as measured by XRF. All values are given in wt%.

Furnace	Al_2O_3	SiO_2	Fe_2O_3	TiO_2	CaO	K_2O	MgO	Density [g/cm^{-3}]	Open porosity [%]
Open	50.8	46.3	1.1	1.6	0.2	0.2	0.1	2.38	16.3
Closed	55.0	42.7	1.0	0.8	0.0	0.4	0.2	2.43	14.2

Table 2: Average chemical composition of regions marked in Figure 6. All values are given in mol%.

Region	Al	Si	O	Na	K	Ca	Mg	Ti
1	6.1	30	63	0.5				
2	22	17	61					
3	33	8	59					
4	20	17	61	0.8	0.5	0.2	0.4	0.7
5	20	17	62	0.2	0.1	0.6	0.3	0.5

Table 3: Average chemical composition for the regions indicated in Figures 8 and 9. All values are shown in mol%.

Region	Al	Si	O	Na	Mg	Fe	Ni	Zn
6	19	0.2	54	1.6	3.4	14	6.6	0
7	1.9	0.6	57	0.8	0.2	36	0.1	2.0
8a	0.8	34	64	0.2		0.1	0.1	0.3
8b	27	9.0	63	0.5	0.3	0.7	0.1	0.4
9	0.8	34	64	0.2				0.3
10	1.9	1.4	64	0.7		31		1.2

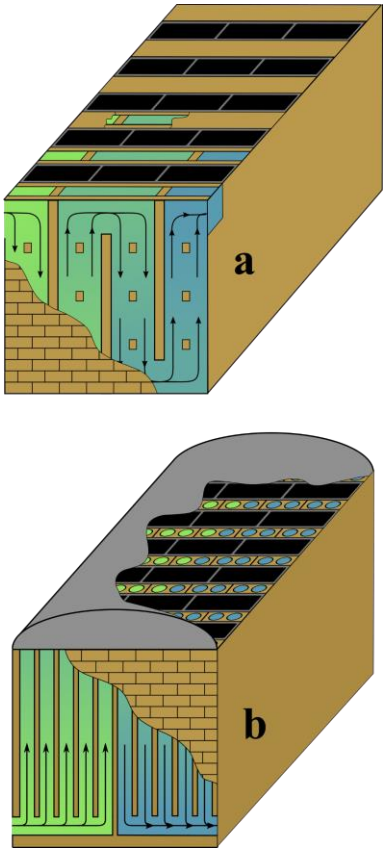

Figure 1: The flue wall cross sections, distribution of flue walls and anode pits are displayed for both a) open and b) closed top baking furnace. The closed furnace flue wall is divided in two parts where part A carries the flue gas upwards (green), while part B transports the flue gas downwards (blue) and into the next section. The gray cover section is illustrated for the closed furnace.

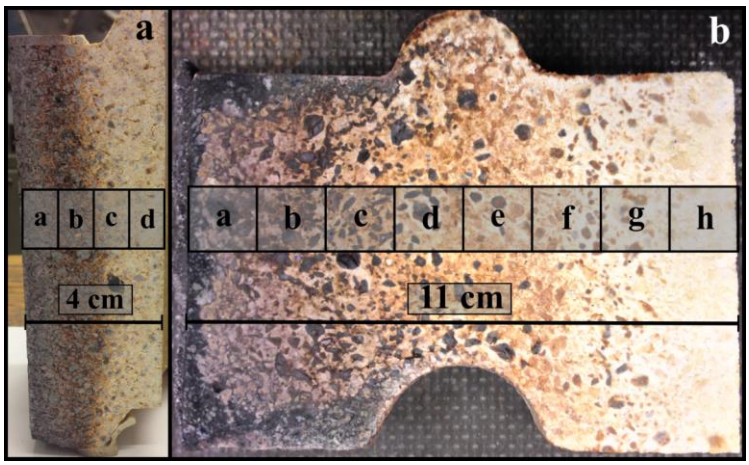

Figure 2: Cross sections of spent lining from both a) closed and b) open furnaces. The left side on both samples have been facing the anode side as indicated by the discoloring.

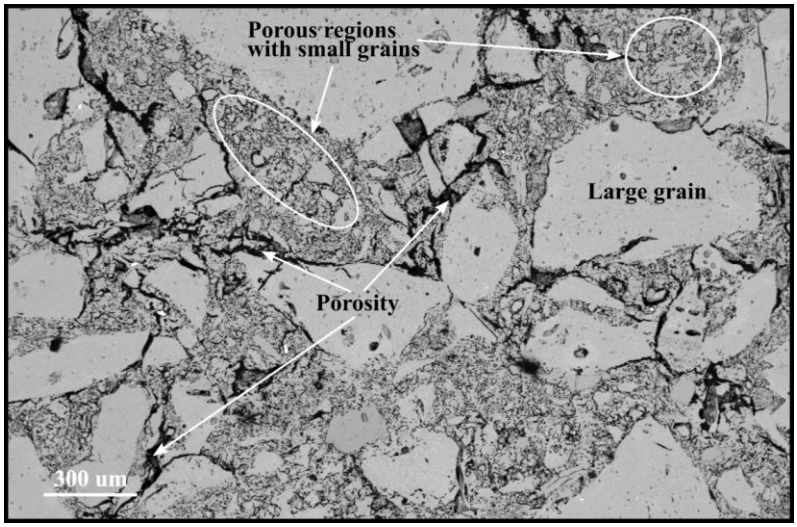

Figure 3: Microstructure of pristine refractory material, illustrating the heterogeneity of the material used in both the open and closed baking furnace. Large grains (bright), porous regions with small grains and pores (dark) are labeled.

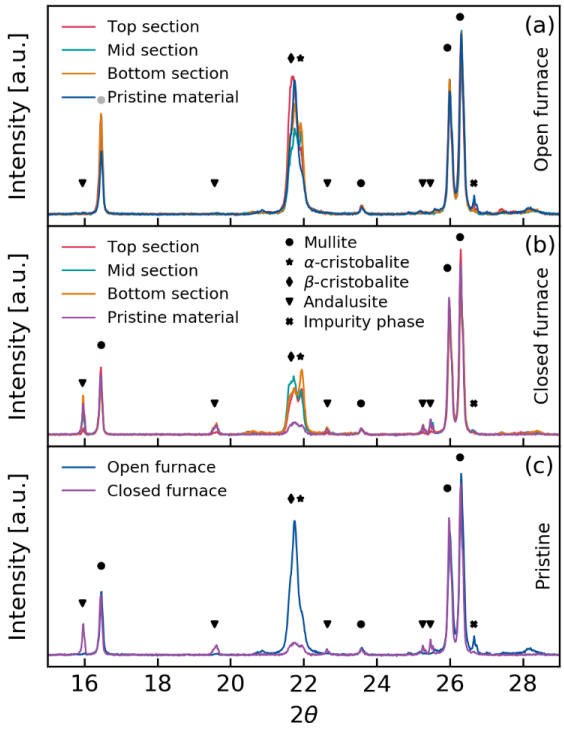

Figure 4: Phase composition of a) samples from the open furnace, b) samples from the closed furnace and c) the two pristine materials. a) and b) include the samples facing the anode pit for all three heights in addition to the pristine materials in c).

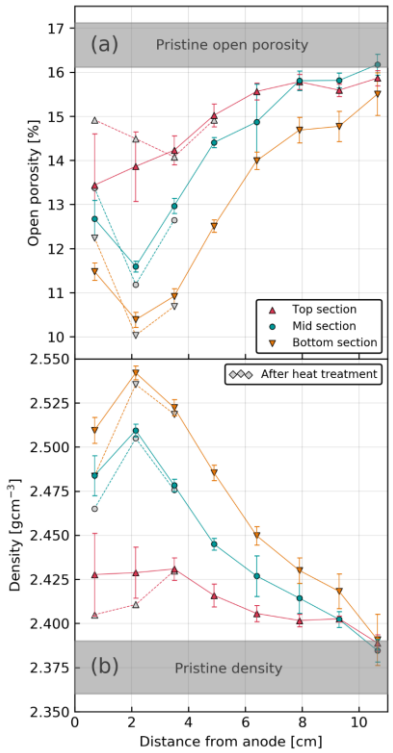

Figure 5: a) Density and b) open porosity of spent lining from the open top baking furnace. Filled and open markers are the density measured before and after heat treatment respectively.

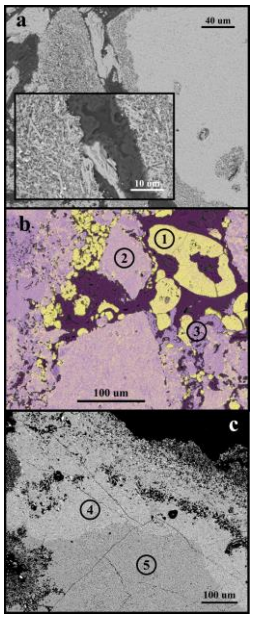

Figure 6: SEM micrographs from the anode facing surface in an open baking furnace. a) Backscatter image of the microstructure of the bottom section, b) EDS image from the top section and c) regions with high and low content of alkali metals from the bottom section. Chemical composition measured at point 1-5 are found in Table 2.

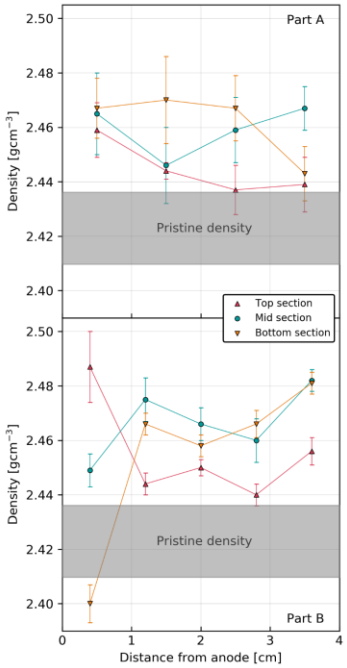

Figure 7: Density of spent samples from a) part A and b) part B of the closed baking furnace.

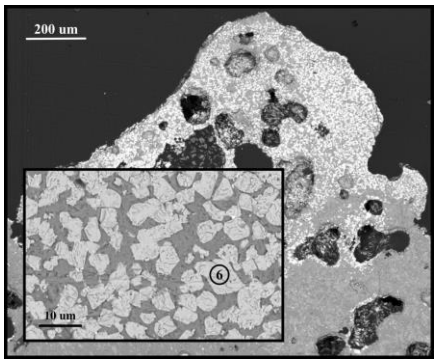

Figure 8: Top section of the closed baking furnace.

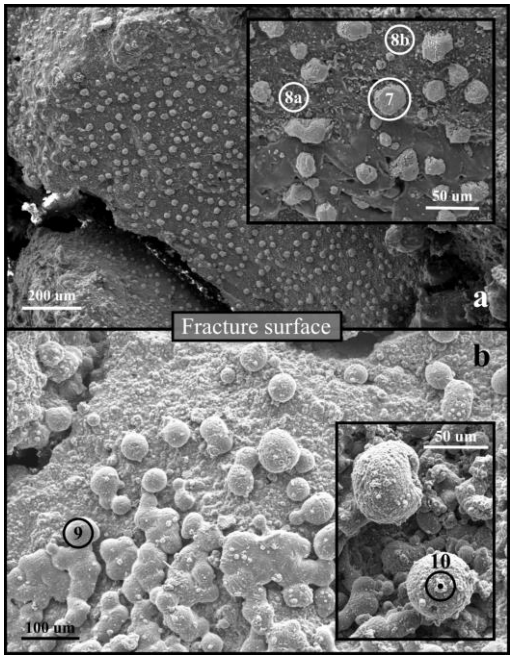

Figure 9: Fracture surface of the bottom section from the closed baking furnace. a) An overview of the surface with the precipitated particles, and b) particles with very high silica content observed in the same region.

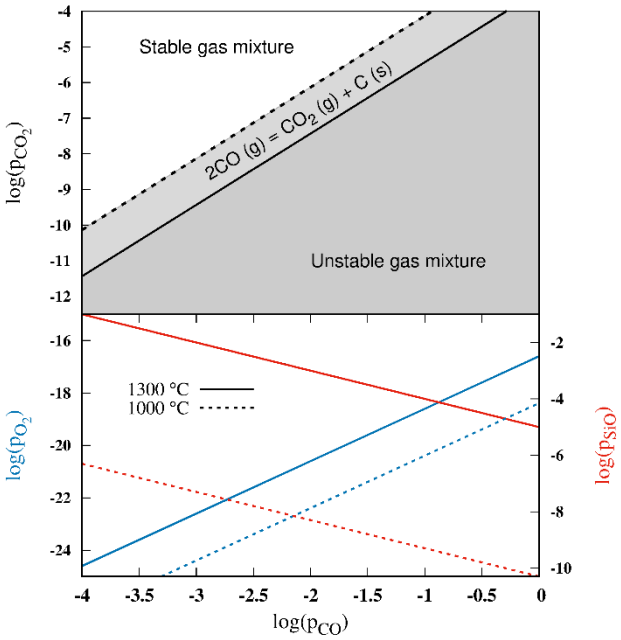

Figure 10: Partial pressures of CO_2, O_2 and SiO plotted as functions of p_{CO}. Pressures for 1300 °C and 1000 °C are presented with solid and dotted lines, respectively. The top section of the figure shows the stability region for the Boudouard reaction, with the equilibrium line separating the two regions.